Performance Optimization of the NASA Large Civil Tiltrotor

C. W. Acree, Jr.[*]   Hyeonsoo Yeo[†]   Jeffrey D. Sinsay[†]
Cecil.W.Acree@nasa.gov   hsyeo@mail.arc.nasa.gov   sinsay@merlin.arc.nasa.gov

Ames Research Center, Moffett Field, California 94035, USA

Abstract

Performance optimization and analysis is presented for a Large Civil Tiltrotor (LCTR2). Intended to replace regional airliners over medium ranges, LCTR2 is designed to carry 90 passengers for 1000 nm or greater, with performance of 300 knots at 28,000-ft altitude. Design features include low hover and cruise tip speeds of 650 and 350 ft/sec, respectively. The paper is primarily concerned with rotor aerodynamic optimization for performance, including rotor/wing interference calculations. Twist, taper, and solidity optimizations are presented, along with an analysis of flight performance in turns. Hover/cruise performance tradeoffs for different cruise tip speeds are also presented. A free-wake model was used for all rotor analyses, computed by the CAMRAD II comprehensive analysis code. Aircraft design was done with the RC sizing code, developed by the U. S. Army Aeroflightdynamics Directorate.

Notation

A	rotor disk area
c_d	section drag coefficient
c_l	section lift coefficient
C_{Lmax}	maximum wing lift coefficient
c_m	section pitching moment coefficient
C_T	rotor thrust coefficient, $T/(\rho A V_{tip}^2)$
C_W	rotor weight coefficient, $W/(\rho A V_{tip}^2)$
D	drag
L/D_e	aircraft lift over equivalent drag, WV/P
L/D_{max}	maximum section lift over drag
FM	figure of merit
M	Mach number
M_{dd}	drag-divergence Mach number
P	power required
q	dynamic pressure
R	rotor radius
t/c	thickness to chord ratio
T	rotor thrust
V	airspeed
V_{br}	aircraft best-range speed
V_{tip}	rotor tip speed
W	gross weight
η	propulsive efficiency
ρ	air density
σ	rotor solidity (thrust-weighted)
ISA	International Standard Atmosphere
JVX	Joint Vertical Experimental
LCTR	Large Civil Tilt Rotor
LRA	LCTR Reference Airfoils
MCP	Maximum Continuous Power
MRP	Maximum Rated Power (take-off power)
OEI	One Engine Inoperative
OGE	Out of Ground Effect
SFC	Specific Fuel Consumption
SLS	Sea-Level Standard conditions
SNI	Simultaneous Non-Interfering approach
VTOL	Vertical Takeoff and Landing

Introduction: Genesis of the LCTR Concept

The NASA Heavy Lift Rotorcraft Systems Investigation was a multidisciplinary study of the technology needs and opportunities for advanced VTOL transports, designed for the short-haul regional market (Ref. 1). The study revealed that a large tiltrotor was the best concept for the mission; the vehicle was designated the Large Civil Tiltrotor (LCTR) and has been documented in several subsequent reports (Refs. 2-7). The concept has since evolved into a more refined design, which makes use of improved design methodologies. To distinguish the different evolutions of the design, this paper uses LCTR to refer to the overall concept, and LCTR1 and LCTR2 to refer respectively to the design developed during the original systems investigation (Ref. 2) and the refined design described herein. The LCTR2 is documented for the first time herein.

The LCTR2 is focused at the short-haul regional market (Fig. 1). It is designed to carry 90 passengers at 300 knots over at least 1000-nm range. It has low disk loading and very low tip speed of 650 ft/sec in hover and 350 ft/sec in cruise. A two-speed gearbox is assumed. Aircraft technology projections from the LCTR1 have been updated for the LCTR2 based on a service entry date of 2018. Table 1 summarizes the nominal mission, and Table 2 lists key design values (the initial values for the current design study).
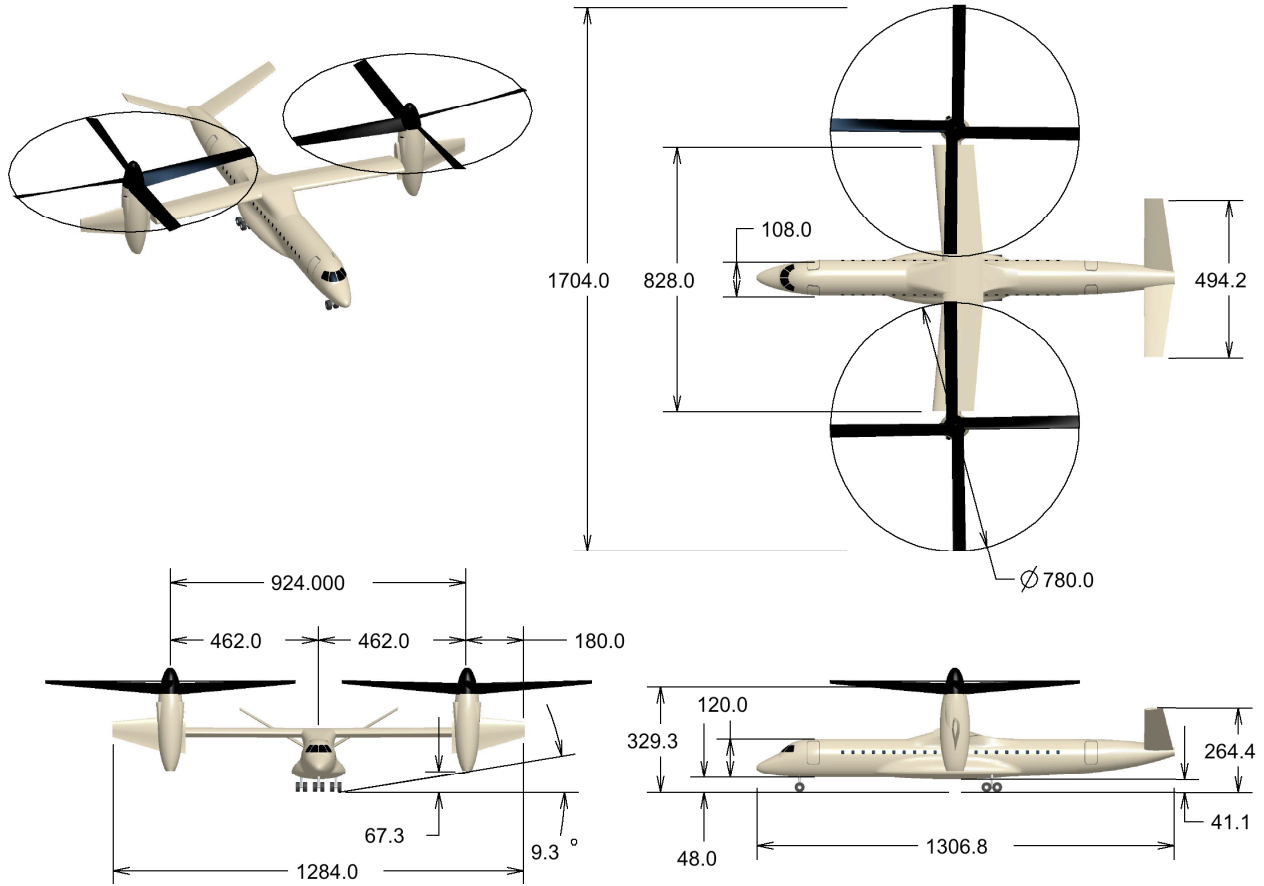
Fig. 1. The NASA Large Civil Tiltrotor, evolved version (dimensions in inches).

Table 1. LCTR notional mission capability.

Mission summary
Takeoff + 2 min hover OGE 5k ISA+20°C
Climb at V_{br} (credit distance to cruise segment)
Cruise at V_{br} for at least 1000 nm range, 28k ISA
Descend at V_{br} (no range credit)
1 min hover OGE + landing 5k ISA+20°C
Reserve: 30 nm + 30 min at V_{br} 28k ISA

Operational requirements
One engine inoperative: Category A at 5k ISA+20°C
All-weather operations: CAT IIIC SNI
45-deg banked turn at 80 knots, 5k ISA+20°C, 90% MCP

The Design Constraint column of Table 2 includes values directly determined by the mission requirements of Table 1, such as payload, and values reflecting the level of technology assumed to be available for production, such as engine SFC. Several design constraint values, notably tip speeds, reflect the results of the LCTR1 design and analysis (Ref. 2) and are the starting points for optimization. Nominal cruise speed is specified as a target value in Table 2, whereas V_{br} in Table 1 is allowed to vary as fuel is burned during the mission. The Baseline Design column summarizes the results of the design synthesis. The process is described in detail in the sections following.

The rotorcraft design software (RC) performs the sizing of the rotorcraft. It includes mission performance analysis, generates airframe and rotor geometry, and calculates overall size, weight, and installed power. RC was developed by the Aviation Advanced Design Office of the U. S. Army Aeroflightdynamics Directorate (AFDD), RDECOM (Ref. 4). RC designs are based upon a physics-based synthesis process calibrated to a database of existing aircraft. The net effect of technology is introduced by projecting non-dimensional improvements in weight and performance parameters, as reflected in the Baseline Design values of Table 2. Table 2 summarizes a design synthesis assuming technology levels consistent with a 2018 entry into service. After initial sizing, rotor performance is checked in detail by the CAMRAD II comprehensive analysis code. CAMRAD II is an aeromechanical analysis for rotorcraft that incorporates a combination of advanced technologies, including multibody dynamics, nonlinear finite elements, and rotorcraft aerodynamics (Ref. 8). Its aerodynamics capabilities include a multiple-rotor free-wake model and rotor/wing interference calculations.

Table 2. Design values for LCTR2.

Design Constraint	Value
Payload (90 pax), lb	19,800
Cruise speed (90% MCP), knots	300
Length, ft	108.9
Wing span, ft	107.0
Wing loading, lb/ft^2	107.4
Wing sweep	−5.0 deg
Engine power, hp	4×7500
SFC (at MRP, SLS), lb/hr/hp	0.373
Rotor radius, ft	32.5
Rotor separation, ft	77.0
Number of blades	4
Precone, deg	6.0
Tip speed, hover, ft/sec	650
Tip speed, cruise, ft/sec	350
Hover C_W/σ	0.133

Baseline Design	Result
Gross weight, lb	107,500
Rotor weight, lb	8756
Wing weight, lb	6505
Engines and drive train, lb	11,872
Cruise SFC, lb/hr/hp	0.375
Mission fuel, lb	20,408
Rotor solidity	0.130
Rotor taper (tip/root chord)	0.7
Hover C_T/σ	0.166
Cruise C_T/σ	0.0867
Disk loading, lb/ft^2	16.2
Wing area, ft^2	1001
Drag D/q, ft^2	33.9

LCTR Sizing Criteria

The LCTR1 was originally designed to a notional mission developed to show the technology pay-off of an advanced rotorcraft that met the Rotorcraft Sector technology goals, as part of the NASA Vehicle Systems Program (Ref. 2). The LCTR1 design mission of carrying 120 passengers to a range of 1200 nm at 350 knots did not properly reflect important real-world considerations in aircraft sizing. The existence of scope clauses, which limit the size of aircraft that can be operated by non-mainline pilots in many airlines, would preclude economical operation of LCTR1 by regional pilots. Current trends in the marketplace point to significant future demand for aircraft seating 80 to 100 passengers. A nominal all-economy configuration of 90 passengers was accordingly established as a design criterion for LCTR2. A 32-in seat pitch and 3×2 seating layout immediately determined the payload and fuselage size in Table 2.

For the LCTR1 design the aircraft design range was fixed and the aircraft installed power and gross weight

adjusted to achieve design closure. In the case of the LCTR2, it was recognized that to be economically feasible the engine should be a derivative design. An engine of the 7500-shp class was identified as being a viable option for LCTR2. Such an engine was assumed to include advanced technology insertion to improve power-to-weight and specific fuel consumption.

A two-speed gearbox was retained, as in the LCTR1 design, to allow for operation of the derivative engine over a typical rpm range. Aircraft take-off gross weight was limited by the same Category A OEI requirement at 5k ISA+20ºC as required for LCTR1. The range of the resultant design was checked to ensure that it did not fall below the target threshold value of 1000 nm.

An emergency maneuver criterion was added, defined as a 1.4-g turn (45-deg bank) at 80 knots, 90% maximum continuous power, at the defined hover condition of 5k ISA+20ºC. The turn was specified as steady state, so that no credit was given for dynamic lift, rotor rpm decay, altitude loss, or other dynamic effects.

LCTR2 also returned to a more conventional high-wing, tilting engine nacelle configuration. The high wing provides better clearance for the engine exhaust when tilted upward for helicopter mode operations. The packaging of engines, transmission, and rotor shaft is more efficiently accomplished with fully tilting engine nacelles than with the fixed engine/tilting rotor configuration explored in the LCTR1 design. Additionally, the LCTR2 wing extends beyond the nacelle with tilting wing extensions, which reduce induced drag by increasing wing span in cruise. The inner wing aspect ratio is increased as compared with LCTR1. The increased aspect ratio, coupled with the vertical orientation of the wing extensions in hover, yields a reduction in download. The assumed net download is 7.4% of gross weight, or 6.9% of rotor thrust. The net jet thrust from the engines also provides some positive vertical force in hover, resulting in a slight improvement in total aircraft hover efficiency.

For LCTR1, the disk loading and wing loading were the results of design optimization with the RC sizing code. In the case of LCTR2, disk loading and wing loading were optimized to higher values, reflecting updates to the technology assessments consistent with the assumed in-service date. C_W/σ (thrust-weighted) is reduced for greater stall margin. The assumed value is derived from V-22 experience. The rotor weight coefficient C_W is appropriate for vehicle sizing, whereas the thrust coefficient C_T is needed for detailed aeromechanics analyses. The distinction is necessary because C_T includes download in hover, which may vary independently of C_W during the sizing analysis.

Blade folding is included, in order to reduce airport gate-space requirements to levels compatible with the

B-737 and A320. This feature is highly desirable for regional airlines that operate into small airports, even at a weight penalty of just under 1000 lb per rotor. Similar considerations limit total wing span, hence rotor radius.

This is merely the starting point for NASA design studies. The relative impacts of different technologies are addressed in this paper, and the results fed back into the sizing and mission analysis code. The intent is not to specify the market or dictate a design, but to identify the potential value of different technologies, which will help guide NASA rotorcraft research.

Design Analysis

For LCTR2, the RC design code determined the design values of Table 2 from the mission specifications of Table 1. CAMRAD II then analyzed the aerodynamics in detail, including performance in turns, rotor/wing interference, and rotor performance optimization. The initial design synthesis by RC resulted in 0.130 solidity, but that provided zero thrust margin in helicopter-mode turns, as analyzed by CAMRAD II. Solidity was increased to 0.150 for better turn performance, then twist and taper were optimized to regain cruise efficiency. Finally, the aircraft was resized, based upon the values of figure of merit and propulsive efficiency for the optimized rotor.

In parallel with the above process, new airfoil tables were constructed to represent state-of-the-art proprotor airfoils. The new tables were applied to LCTR2 rotor optimization to define the final performance baseline. Starting from this baseline, variations in tip speed and airfoil thickness were analyzed to determine the most appropriate combination for the next round of optimization, and ultimately the most productive direction of future research. The steps of the design process are discussed in detail in the sections following.

The focus here is on aerodynamics analyses for performance optimization. The blade and wing structure are scaled from LCTR1 (structure designed by Penn State, Ref. 9), and an equivalent beam-element rotor structural model is included in CAMRAD II. The engine and drive-train technology is based on LCTR1 (Ref. 2) and incorporated into the RC model.

CAMRAD II Model

CAMRAD II is a comprehensive rotorcraft analysis code (Ref. 8), with a free-wake model, a multi-element structural beam model, and a choice of stall delay models. It is much more computationally efficient than any equivalent CFD/CSD code. CAMRAD II is, therefore, well-suited for rotorcraft design optimization where efficient aeromechanics analysis is needed.

The CAMRAD II rotor model of the LCTR2 had five elastic beam elements per blade, with full control-system kinematics, and 15 aerodynamic panels per blade. Blade aerodynamics were modeled as a lifting line coupled to a free-wake analysis. An isolated-rotor, axisymmetric solution was used for hover and cruise performance optimization. For turn performance, the complete aircraft was modeled, including rotor and airframe aerodynamics, with a non-symmetric free wake for each rotor. The rotor/wing interference model incorporated a wake model for the wing in addition to the rotor wakes.

Blade-section aerodynamic properties were read from 2-D coefficient tables (discussed in more detail in the next section). Rotating, 3-D stall delay was implemented as modifications to the 2-D aerodynamic table data, based on the analysis of Ref. 10.

The CAMRAD II rotor model for LCTR2 evolved from the JVX rotor model of Refs. 11 and 12. The JVX rotor was an experimental precursor to the V-22 rotor. Its test history and relationship to the production V-22 rotor are discussed in Ref. 11. Validation of the CAMRAD II JVX model against experimental data is described in Ref. 11 for both hover and cruise conditions. Development of an inflow model (wake model) appropriate for design optimization is described in Ref. 12.

To create the LCTR2 analytical model, the CAMRAD II model for JVX was modified to include four blades, then scaled up to LCTR2 diameter and solidity. The blade structure is an adaptation of that developed for LCTR1 (Refs. 2 and 9). The last step was to replace the JVX airfoil tables (XN-series airfoils, Ref. 13) with newly-developed tables.

Airfoil Technology

It is desirable to include airfoils as an additional dimension of the design space. The immediate motivation is to trade tip airfoil thickness against tip speed. However, incorporating airfoils into rotor optimization presents a dilemma: rigorous airfoil design requires knowledge of the local flow conditions, but varying tip speed (for example) changes those conditions. This expands the airfoil design matrix to an impractical size.

To address this problem, airfoil coefficient tables were constructed directly, based upon projected improvements beyond existing airfoil capabilities. These projections were based on CFD analysis and modern rotor airfoil trends. This approximates the results of a full airfoil design effort, parallel in concept to the technology projection utilized by RC. The "virtual airfoils" represented by these tables simulate performance levels expected of state-of-the-art, purpose-designed airfoils (see Refs. 14 and 15 for examples applicable to LCTR1). The LCTR2 Reference Airfoil (LRA) tables were constructed

to be generally compatible with XN-series characteristics (Ref. 13), with slight performance improvements consistent with more modern airfoils.

Although not as rigorous as actual airfoil design and test, this procedure ensured consistent variations of airfoil properties, and therefore reliable determination of performance trends. Detailed airfoil design can then proceed with assurance that the airfoil design specifications are consistent with the optimum rotor design.

Table 3 summarizes the airfoil performance targets and compares them to the XN-series airfoils used on the JVX rotor. The airfoils are designated by their nominal t/c (e.g., LRA-09 is 9% thick). The coefficients at $M = 0.0$ are extrapolated from low airspeeds.

Figure 2 compares the Mach number distribution along the rotor blade for the critical LCTR2 operating conditions of Table 1. The airfoil radial locations, in order of decreasing t/c, are 0.225, 0.50, 0.75, and 1.00 R (the same as the JVX test rotor, Ref. 11).
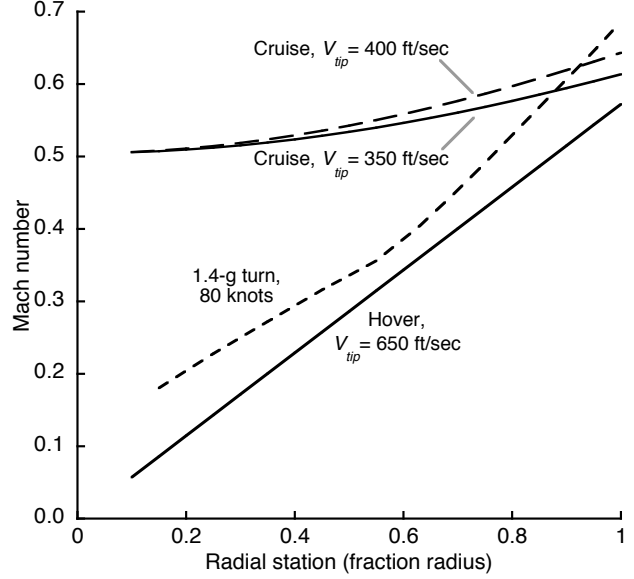

Fig. 2. Blade section Mach distribution for hover, cruise and 80-knot turn.

Baseline Performance

Figures 3 and 4 compare hover and cruise performance for the XN and LRA airfoils. The LRA airfoils give performance trends similar to that of the XN airfoils, but with slightly better performance at the hover and cruise design points (hover $C_T/\sigma = 0.166$, cruise $C_T/\sigma = 0.0867$ at 300 knots). The LRA airfoils have better performance margin at high thrust in hover, but no improvement at very high speeds. For Figs. 3 and 4, the rotor twist was optimized separately for the two airfoil families to avoid biasing the results.
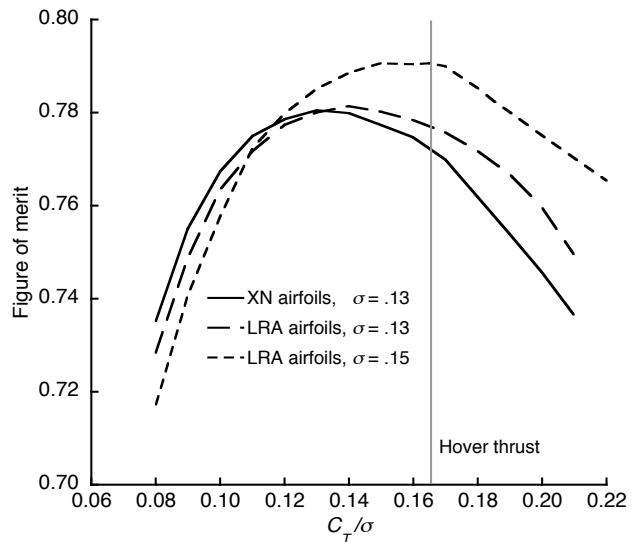
Table 3. Airfoil performance comparison (Ref. 13).

Performance goal	XN09	LRA-09
$c_{l\max}$	1.35, $M = 0.6$	1.15, $M = 0.5$
c_d @ $c_l = 0.3$	0.006 @ $M = 0.75$	0.006 @ $M = 0.6$
c_m @ $M = 0.0$	-0.02	-0.026
M_{dd} @ $c_l = 0.3$	0.81	0.76
Hover $L/D_{\max}$	80 @ $M = 0.65$	90 @ $M = 0.55$
	XN12	LRA-12
$c_{l\max}$	1.40, $M = 0.45$	1.40, $M = 0.4$
c_d @ $c_l = 0.2$	0.006 @ $M = 0.65$	0.007 @ $M = 0.60$
c_m @ $M = 0.0$	-0.03	-0.02
M_{dd} @ $c_l = 0.2$	0.72	0.72
Hover $L/D_{\max}$	95 @ $M = 0.5$	90 @ $M = 0.4$
	XN18	LRA-18
$c_{l\max}$	1.5, $M = 0.3$	1.7, $M = 0.3$
c_d @ $c_l = 0.0$	0.007 @ $M = 0.57$	0.007 @ $M = 0.55$
c_m @ $M = 0.0$	-0.05	-0.05
M_{dd} @ $c_l = 0.0$	0.64	0.69
Hover $L/D_{\max}$	80 @ $M = 0.3$	90 @ $M = 0.3$
	XN28	LRA-28
$c_{l\max}$	1.35, $M = 0.19$	1.3, $M = 0.15$
c_d @ $c_l = 0.0$	0.018 @ $M = 0.51$	0.013 @ $M = 0.5$
c_m @ $M = 0.0$	-0.12	-0.08
M_{dd} @ $c_l = 0.0$	0.59	0.61
Hover $L/D_{\max}$	50 @ $M = 0.2$	80 @ $M = 0.2$

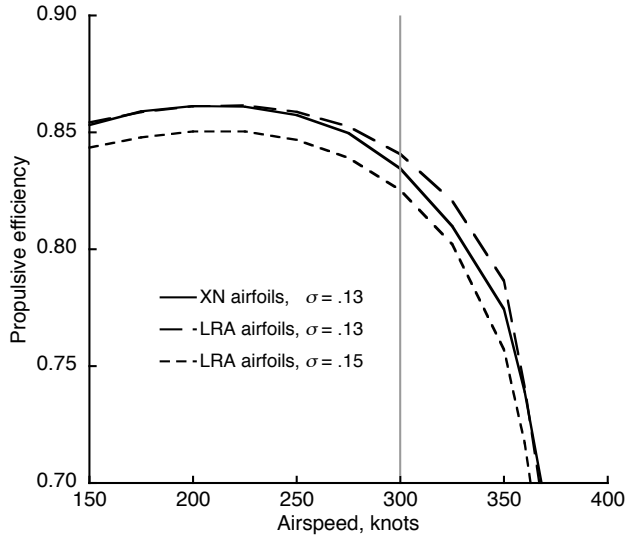Fig. 3. LCTR2 hover performance, comparing XN to LRA airfoils.

Fig. 4. LCTR2 cruise performance, comparing XN to LRA airfoils for V_{tip} = 350 ft/sec.

Although the LRA airfoils often exhibit lower performance individually than the XN goals (Table 3), the overall rotor performance is actually improved at the LCTR2 design points because the airfoils are better matched to its slower tip speeds (650 ft/sec vs. 754 ft/sec in hover, 350 ft/sec vs. 643 ft/sec in cruise). The figures also show the impact on performance of increased rotor solidity, which was added to improve turn performance (discussed in the next section).

Rotor Optimization

Once the baseline design was established by the sizing code RC, rotor performance was examined in detail by the comprehensive aeromechanics code CAMRAD II. Performance in turns was checked to determine adequate rotor solidity, and taper and solidity were then optimized together to determine the tradeoff between hover and cruise performance. Rotor twist was optimized for the selected taper and solidity. Wing and tip-extension optimization is discussed later in a separate section, Rotor/ Wing Interference.

Solidity, taper and twist optimizations were repeated to ensure consistent assumptions at the conclusion. Twist was optimized for the solidity and taper chosen for acceptable turn performance. Solidity and taper were then reoptimized and the turn analysis rerun using the new twist distribution. In principle, this process could be iterated several more times for even better performance. However, performance gains were marginal after the first two optimization cycles. Moreover, the results at this stage are sufficiently converged to have important implications for both the design process and rotor technology. These issues are discussed in the Recommendations section at the end of this paper.

Turn Performance

Although turn performance was analyzed for LCTR1 (Ref. 2), it was not an explicit requirement; its inclusion herein therefore merits discussion. In the design of tiltrotor aircraft, it is desirable to have a continuous maneuver capability during all phases of flight. This maneuver capability can be represented by the ability of the aircraft to generate positive load factors in helicopter mode, airplane mode, and conversion. In airplane mode, the wing provides the primary means of generating positive load factor. Increasing dynamic pressure increases the maximum lift that can be generated by the wing and so determines the obtainable load factor. In helicopter mode, the rotor provides the primary means of generating positive load factor. As with helicopters, the obtainable load factor for a tiltrotor when rotor-borne decreases with speed as retreating blade stall and advancing tip Mach number reduce the maximum thrust the rotor can generate.

During conversion, positive load factor is generated by a combination of rotor thrust and wing lift. The wing lift is limited to some value less than the total gross weight by wing C_{Lmax}, and the effective contribution of the rotor to load factor decreases as the nacelle is tilted forward. The critical case for maneuvers occurs in the conversion region, where will be found the worst-case limit to the load factor that the tiltrotor can generate. It is therefore desirable to identify a criterion in this region that will effectively ensure the stated goal of continuous maneuver capability. This translates into a sizing condition for blade loading because wing span and aspect ratio, hence wing loading, are constrained by other factors in the design of tiltrotors.

During low-speed (80 knots) forward flight, the ability to generate 45-deg banked turns is desirable for obstacle avoidance and maneuvering during approach and departure near congested airports. Present tiltrotor operational and design experience indicates the desirability to operate at such speeds with a slightly forward nacelle tilt of 60 deg. Based upon these criteria, blade loading was adjusted so that LCTR2 could perform a 45-deg banked turn at 80 knots and 60-deg nacelle tilt, requiring no more than 90% MCP to maintain level flight. The power margin was added so that the pilot would retain the ability to continue acceleration and conversion to airplane mode while maneuvering if conditions warranted.

In order to assess the 45-deg banked turn maneuver capability of LCTR2, a load factor sweep was conducted at 80 knots with 60-deg nacelle tilt. The turn rate was progressively increased to achieve a load factor of 1.41g with 650 ft/sec tip speed at 5k ISA+20°C. At these conditions, 90% MCP equals 15,600 hp. The CAMRAD II analysis was conducted using nonuniform

inflow with a free-wake geometry and full aircraft trim, including wing/rotor lift sharing.

Figure 5 shows the aircraft power versus load factor, using the LRA airfoils. The baseline design with $\sigma = 0.13$ barely meets the maneuver requirement (the intersection of available power and target load factor). However, the slope of aircraft power curve quickly steepens above a load factor of 1.3 due to stall. If the rotor is partially stalled, it may not be possible to generate additional thrust for acceleration even with a generous power margin. Increasing solidity to 0.15 alleviates stall, which significantly reduces aircraft power required at high load factors. With the XN airfoils, the trend in turn performance was nearly identical for $\sigma = 0.13$, but with a 5.1% increase in power required at 1.41g.
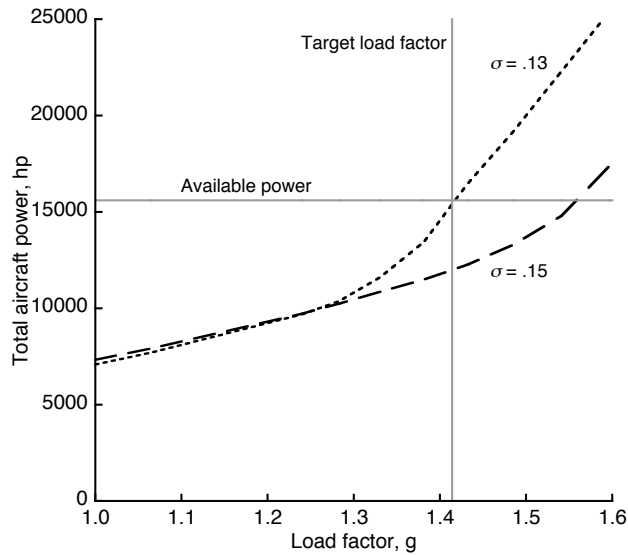
Fig. 5. Power required for an 80-knot turn.

Solidity/Taper Optimization

Figure 6 summarizes the results of the solidity and taper optimization, plotted as figure of merit (*FM*) and propulsive efficiency (η). A large matrix (8×7) of combinations of solidity and taper defines the design space. The twist distribution was fixed at −38 deg/*R* inboard of 0.5 *R* and −30 deg/*R* outboard. The tradeoff between hover and cruise performance is nearly linear, and follows the outermost boundary of the overlapped curves. However, if solidity is fixed by thrust (or power) margin in turns, then the tradeoff is locally nonlinear, with a distinct corner at maximum *FM* for each value of solidity. Best cruise performance requires minimum taper (driven by root drag), whereas best hover performance requires 0.75-0.80 taper.
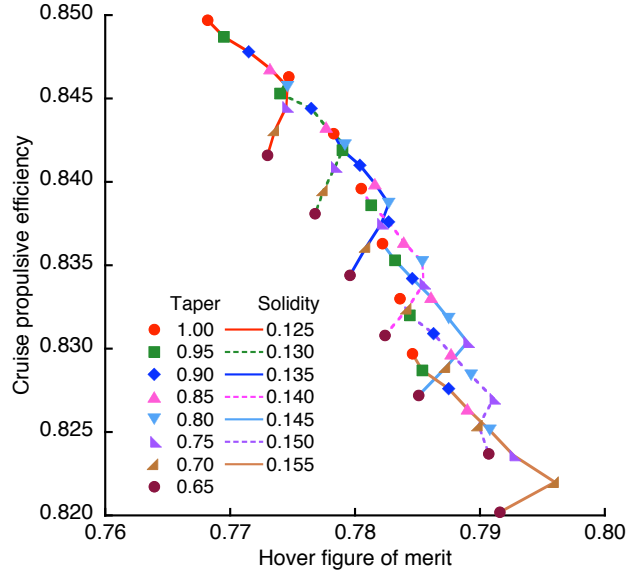

Fig. 6. Taper/solidity optimization map for nominal tip speeds and fixed twist.

For LCTR2, taper was set to 0.70 for lower rotor weight. Figure 6 indicates that there is an opportunity for a small further improvement in performance with slightly less taper. However, a rigorous reoptimization of taper would include structural weight costs, hence at least one new dimension in the design space. Reference 16 suggests that inverse or compound taper should be beneficial, but this would entail further structural design challenges well beyond the scope of the present study.

Twist Optimization

The CAMRAD II rotor model was next applied to bilinear twist optimization. Bilinear twist applies a constant twist rate from the blade root to a given transition radius, then a different rate to the tip. This is the classic compromise for proprotors which must have good performance in both hover and high-speed cruise. For the LCTR2, the transition radius was 0.50 *R*.

Figure 7 shows a conventional twist optimization map for combinations of inboard and outboard linear twist. A matrix (7×7) of combinations of inboard and outboard twist rates was analyzed to map the design space. Cruise conditions favor lower inboard twist than does hover, although both require outboard twist near −30 deg/*R*. There are fewer practical design constraints upon blade twist than upon planform, so twist was varied more freely than solidity or taper. The effect can be seen in the larger variation in η in Fig. 7 (twist) than in Fig. 6 (taper/solidity).
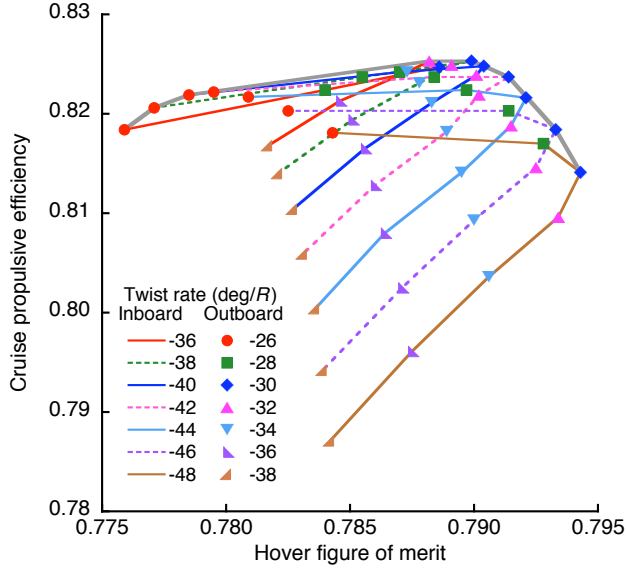
Fig. 7. Example twist optimization map for nominal tip speed, $\sigma = 0.15$.

The outer envelope of the twist map is also drawn on Fig. 7. The optimum combination of inboard and outboard twist lies somewhere on this boundary. In principle, the optimum could be determined by a performance function applied to points along the boundary (for LCTR1, the function was simply an estimate of mission fuel burn). However, LCTR2 cruise performance has already been reduced by increasing solidity to meet the turn requirement, so here the twist was determined by peak η in order to recover as much cruise performance as possible. The optimum twist distribution thus found was -38 deg/R inboard and -30 deg/R outboard.
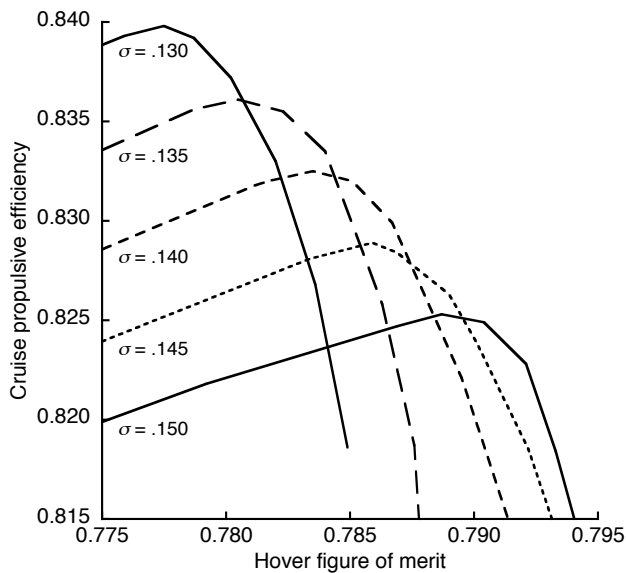
Fig. 8. Twist map boundaries for different rotor solidities at nominal tip speed.

A different view of the tradeoff of hover versus cruise performance is given in Fig. 8. Here, only the optimization boundaries of several twist maps are shown, one for each value of σ. Thrust is held constant at the nominal hover and cruise values (Table 2) as σ is varied. Five different dimensions—inboard twist, outboard twist, σ, FM, and η—are projected onto the two performance dimensions of the plot. The tradeoff between hover and cruise performance is nearly linear along the outermost boundaries of the overlapped curves, but the tradeoff for any given value of σ is nonlinear.

In contrast to Fig. 6, where the twist distribution was fixed, Fig. 8 includes variations in both twist and σ, taper was fixed at 0.7. This emphasizes the result that, for the specified values of C_T (Table 2), figure of merit increases with increasing σ, and propulsive efficiency decreases.

Rotor/Wing Interference

Aircraft performance calculations were conducted at various speeds to examine the rotor/rotor and rotor/wing interference effects. Rotor/rotor and rotor/wing interferences were accounted for using a vortex wake model. The wing free-wake model consists of a vortex lattice in the near wake behind the wing with 32 aerodynamic panels, rolling up to tip vortices (with shed wake panels between) in the far wake. The wing wake includes the tip extensions. Thus, comparable models were used for both wing and rotor wakes in this investigation of the interference. Solidity was set to 0.150, and the twist set to the value resulting from twist optimization (Fig. 7). The analytical method is described in detail in Ref. 17; see also Ref. 5.

The interference effect increased aircraft L/D_e at the speed range investigated as shown in Fig. 9, a known effect with this rotor rotation (outboard down). The interference effect reduced wing induced power and thus improves aircraft L/D_e, which was reported in Ref. 17. The most beneficial effect (4.8% increase of aircraft L/D_e) was observed at 250 knots. At the design cruise speed of 300 knots, L/D_e improved from 11.2 to 11.6, a 3.6% increase.

Figure 10 shows the effects of wing-tip extension incidence on aircraft performance at 300 knots. The baseline design has a 3.3-deg incidence angle for both the wing and the tip extensions. The tip extension incidence was varied by ±2 and ±4 deg to examine its influence. In general, the tip extension incidence has very small influence on the aircraft performance; note the greatly expanded scale of Fig. 10 compared to Fig. 9. The maximum change in L/D_e was −2.8% from the baseline with a −4-deg change in incidence. The result shows that the baseline value was optimum for the current aircraft.
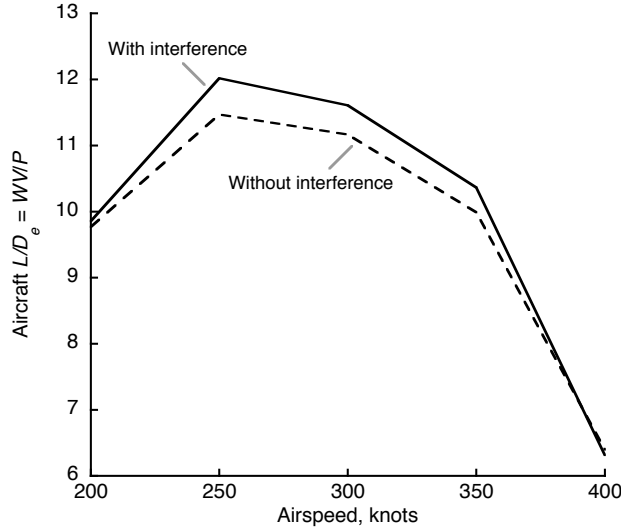
Fig. 9. Effect of wing/rotor interference on cruise performance, $\sigma = 0.150$.
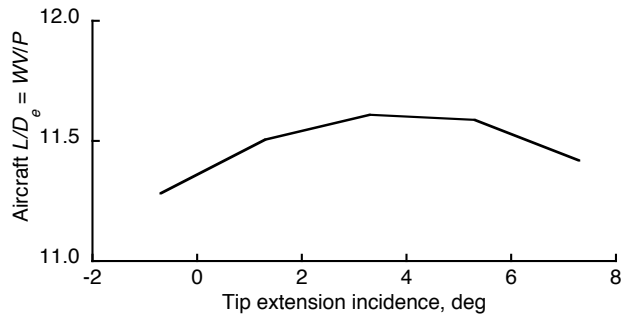

Fig. 10. Effect of tip extension incidence angle on cruise performance, $\sigma = 0.150$.

LCTR2 Performance Update

As a result of the rotor aeromechanics analyses, the aircraft design was updated. The first step was to recalibrate the RC rotor model against the CAMRAD II calculations of rotor performance. This included the effects of increased rotor solidity: increased stall margin in turns, better hover *FM*, and reduced cruise η. After RC was updated, the aircraft was resized to regain some of the range lost because of reduced η.

Because solidity was increased in order to achieve more stall margin during turns, there was a significant reduction in propulsive efficiency, even after reoptimizing twist. Table 4 summarizes the net effect on performance as calculated using RC calibrated to the CAMRAD II results for rotor optimization. The Baseline column includes relevant values from Table 2, plus the assumed rotor *FM* and η (uncalibrated). The baseline values of *FM* and η were derived from V-22 performance. The Rotor Update column has the rotor performance values for the higher-solidity rotor ($\sigma = 0.15$) and LRA airfoils. The Wing Mod

column has results for longer tip extensions, added to recover some of the range lost when the rotor was resized. Engine size was fixed at 4×7500 hp.

The cruise L/D_e shown in Table 4 includes drive system and accessory losses not included in the aero optimization shown Fig. 9. Additionally, the positive rotor/wing interference effect seen in CAMRAD II analyses was not fully captured in the RC resizing.

The reduction in range with the larger rotor is significant, and highlights the extreme sensitivity of long-range tiltrotors to cruise efficiency. With the longer wing, mission fuel required has also decreased, but by a smaller percentage than range. The Wing Mod update attempted to recapture some of the cruise efficiency by reducing induced drag. However, wing span was limited to less than 118 ft, to keep the vehicle within the FAA Aircraft Design Group III limit (for B-737/A320 gate compatibility) with the rotors folded.

Figure 5 suggests that the resized rotor has an overly generous performance margin in turns, and Fig. 9 indicates that the value of L/D_e assumed by RC is too conservative. Moreover, additional performance can be regained in both cruise and hover by reoptimizing tip speed, as discussed in the next section.

Table 4. LCTR2 design updates after resizing the rotor for turn performance.

	Baseline	Rotor Update	Wing Mod
Gross weight, lb	107,500	107,700	107,725
Range w/ 90 pax, nm	1,246	972	1,038
Rotor weight, lb	8,756	9,803	9,805
Wing weight, lb	6,505	6,641	7,010
Mission fuel, lb	20,408	18,154	17,790
Rotor solidity	0.13	0.15	0.15
Hover *FM*	0.787	0.790	0.790
Cruise η	0.870	0.825	0.825
Cruise L/D_e	10.1	9.3	9.9
Wing span, ft	107	107	117
Wing area, ft^2	1,001	1,001	1,061
Drag D/q, ft^2	33.9	34.2	34.7

Design Excursions

Two sets of design excursions were explored in an attempt to regain the cruise performance lost when the rotor blade area was increased. Varying cruise tip speed gave significant results, which are discussed in some detail immediately following. Varying airfoil thickness gave mixed results, summarized at the end of this section.

Cruise Tip Speed

It was anticipated that reducing tip speed in cruise would increase propulsive efficiency through two effects. As tip speed is reduced, the lower dynamic pressure reduces blade profile drag and increases section c_l for the same integrated thrust. As long as the blade sections operate in their design angle of attack ranges, section lift-to-drag ratio should increase, with a resulting improvement in overall performance.

However, for the LCTR2, optimum cruise V_{tip} proved to be higher than expected. Figure 11 summarizes the benefit of increased V_{tip}. Because the section speeds are changing, twist must be reoptimized for each combination of hover and cruise tip speeds. Here, hover tip speed was held fixed at 650 ft/sec, and cruise C_T was varied to maintain constant thrust. Optimum cruise V_{tip} is about 400 ft/sec. Figure 2 compares section Mach numbers for nominal and increased V_{tip}. Hover performance also increases for higher cruise V_{tip} because the optimum cruise twist better approximates the optimum hover twist. The net effect on η and FM may be small, just over 1% each, but even tiny improvements to efficiency can add up to significant reductions in gross weight for a long-range aircraft.

All analyses in this section are based on $\sigma = 0.15$, as required for turn performance, and include the LRA airfoils.
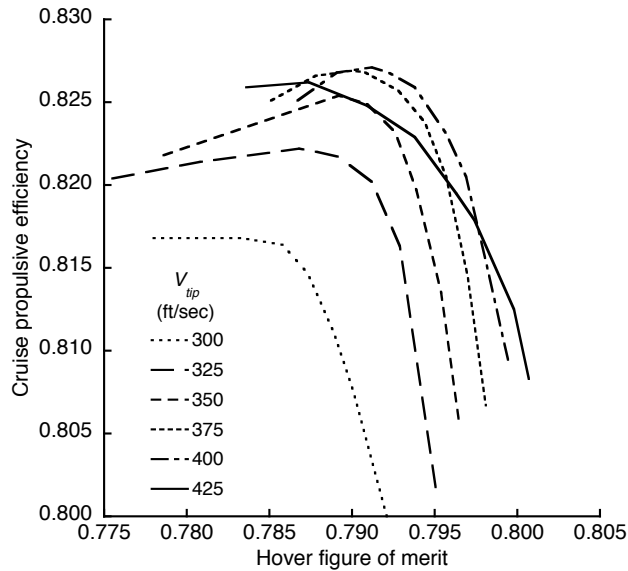

Fig. 11. Twist map boundaries for different cruise tip speeds, $\sigma = 0.150$.

Figure 12 shows the blade section thrust (force per unit length, in the direction of flight). The curves for different tip speeds collapse upon each other, illustrating that the section lift integrates to the same total thrust, and that the effect of tip speed on radial lift distribution is small.
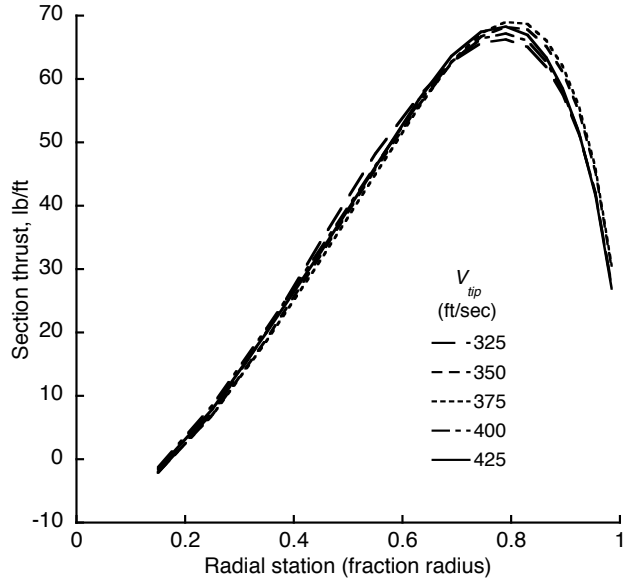

Fig. 12. Blade section thrust for different cruise tip speeds, $\sigma = 0.150$.
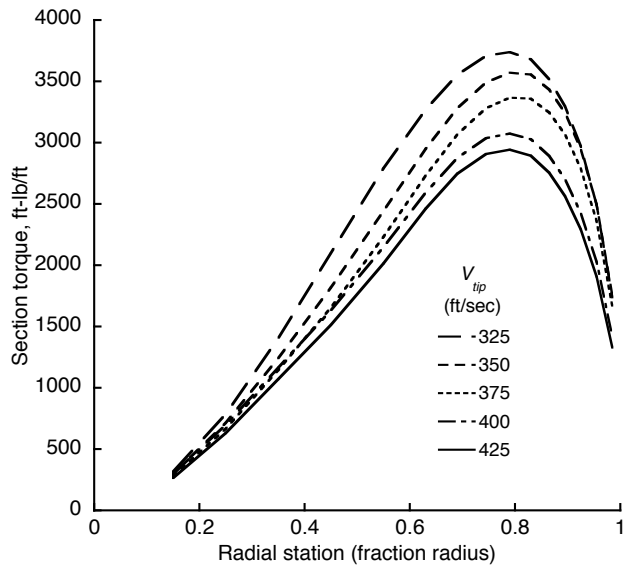

Fig. 13. Blade section torque for different cruise tip speeds, $\sigma = 0.150$.

The equivalent plot for section drag is shown in Fig. 13, here in units of section torque (drag × radius), as appropriate for comparing the effect of drag on power. Figure 14 replots drag as section power (drag × the local in-plane velocity component). Again, the curves collapse, with a common trend very similar to that for thrust (Fig. 12).

The effects of tip speed on thrust and power, hence efficiency, are small and difficult to discern at the scales of Figs. 12-14. In contrast, Fig. 15 shows the distinct changes in section angle of attack at different tip speeds. Close examination reveals that twist is not consistently optimized for $V_{tip} = 400$ ft/sec. The larger issue, however,

is that the angle-of-attack distribution is not merely shifted or scaled as V_{tip} changes, but subtly changes shape; the same effect can be seen for section torque in Fig. 13. Very small changes in section angle of attack lead to changes in both drag and induced velocity, which although small, integrate to significant changes in overall efficiency. The twist distribution was subsequently adjusted to smooth out the angle-of-attack trends of Fig. 15, but this had little effect on the optimum tip speed. Nevertheless, a more sophisticated twist optimization procedure should improve efficiency, especially if coupled to a simultaneous optimization of tip speed.
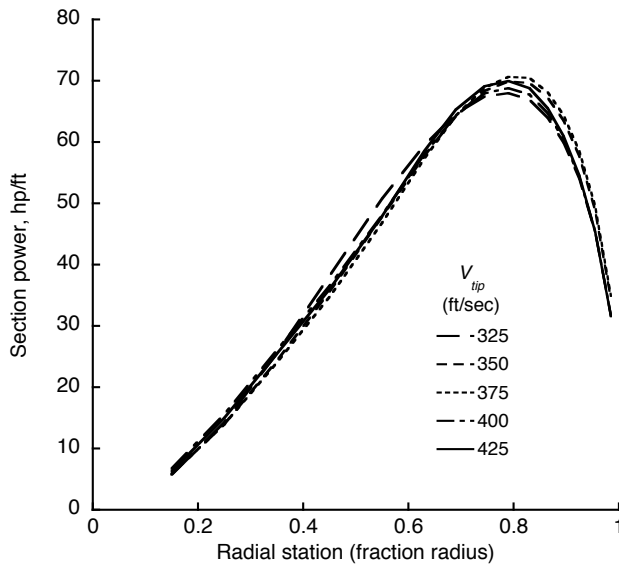

Fig. 14. Blade section power for different cruise tip speeds, $\sigma = 0.150$.
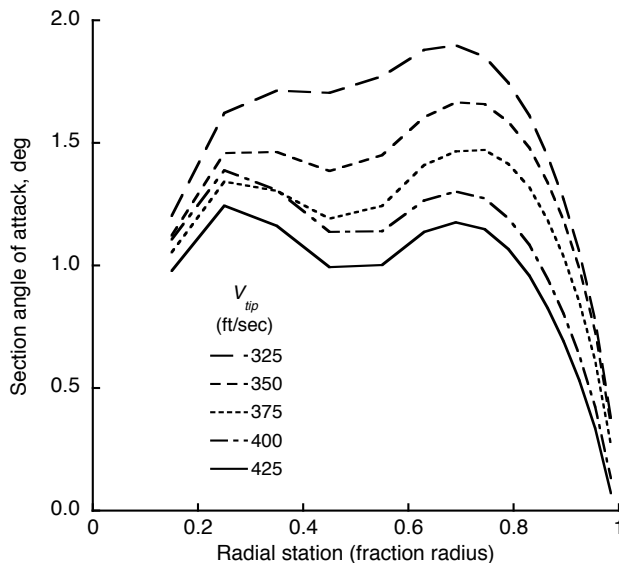

Fig. 15. Blade section angle of attack for different cruise tip speeds, $\sigma = 0.150$.

Rotor Airfoil Thickness

The effects on performance of blade airfoil thickness were also examined. Figure of merit and propulsive efficiency were calculated as airfoil thickness was reduced at the tip and root separately. Solidity was set to 0.150, V_{tip} was held at the nominal values of Table 2, and twist was fixed at the optimum value of Fig. 7. Changes in airfoil thickness were simulated by linear interpolation between airfoil tables.
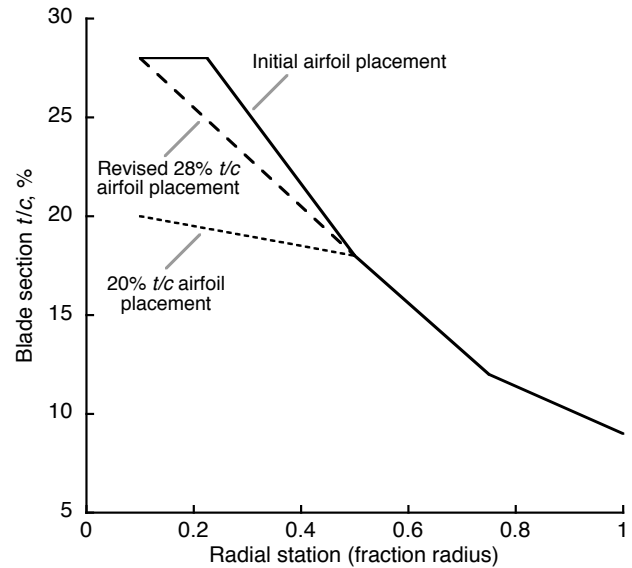

Fig. 16. Blade airfoil section placement.

Figure 16 plots the radial thickness distribution. The original design placed the LRA-28 at 0.225 R to match the JVX rotor; the thickness was constant from 0.225 R inboard to 0.10 R (the start of the blade aerodynamic surface). For the investigations described in this section, the inboard airfoil was moved to 0.10 R to better model a modern, hingeless hub. For both versions, the LRA-18 airfoil was placed at 0.50 R, the LRA-12 at 0.75 R, and the LRA-09 at the tip. The CAMRAD II analysis linearly interpolated the airfoil properties between the defined radial locations.

To analyze the sensitivity to root thickness, the innermost airfoil was progressively reduced in thickness from 28% to 20%, with a large consequent improvement in propulsive efficiency (Fig. 17). Figure 16 illustrates the most extreme values of inner airfoil thickness, which correspond to the ends of the trend line in Fig. 17. Thinning the inner airfoil results in an impractical thickness distribution over the mid-span, but it emphasizes the differences between root and tip thickness effects.

The sensitivity of cruise performance to thickness was almost perfectly linear. In contrast, the effect on hover performance was minimal: figure of merit improved from 0.793 to 0.795 as the inner airfoil thickness decreased

from 28% to 20%. This implies that the decrease in drag was slightly more beneficial than the decrease in maximum lift. A thinner root would be structurally challenging, or at least heavier, but the payoff in propulsive efficiency is potentially large. The structural penalty could potentially be reduced with a nonlinear distribution (in effect, by shifting the entire airfoil distribution inboard, not just the thickest airfoil).
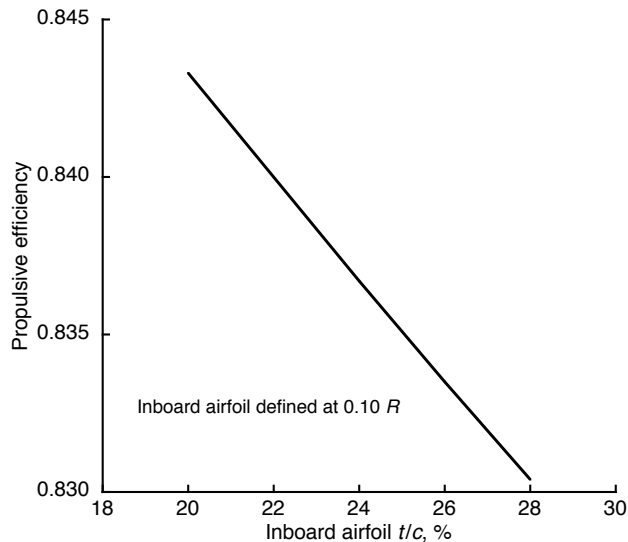

Fig. 17. Effect of inboard airfoil thickness on cruise performance, $\sigma = 0.150$.

In a separate analysis, blade tip thickness was increased from 9% to 12%, in hopes of improving hover performance, and with the expectation that the relatively low tip speed would mitigate the reduction in cruise performance. However, there were very slight decreases in *FM* and η, both by 0.002, with most of the decrease occurring at 12% *t/c*. Given that cruise performance would benefit from increased tip speed (Fig. 11), and that increased tip thickness does not help in hover, it is unadvisable to increase tip thickness.

The results seen here appear to mirror those of Ref. 18, where the tip and mid-span airfoils were considered adequate, but the root airfoil was redesigned. However, there has yet to be an explicit examination of the tradeoffs between airfoil thickness and tip speed. A revised, nonlinear airfoil distribution would alleviate the structural penalties of a thin root, and slightly thicker airfoils might improve turn performance enough to allow a reduction in solidity.

Conclusions

Following the success of the NASA Heavy Lift Rotorcraft Systems Investigation, an updated Large Civil Tiltrotor (LCTR2) was designed to complement regional airliners. Specified to carry 90 passengers for 1000 nm minimum range, its cruise speed is 300 knots at 28,000 ft altitude. It has low hover and cruise tip speeds of 650 and 350 ft/sec, respectively.

The baseline design was generated by the RC sizing code. Twist, taper, and solidity were optimized, turn performance was analyzed, and rotor/wing interference was calculated. Hover/cruise performance tradeoffs for different cruise tip speeds were determined. All aeromechanics analyses were performed with the CAMRAD II comprehensive code.

The effect of rotor/wing aerodynamic interference was slightly beneficial to cruise efficiency. The optimum tip-extension incidence angle was the same as the wing (3.3 deg), including interference effects.

The optimum cruise tip speed proved to be higher than expected, apparently because of subtle changes in blade load and torque distribution. Bilinear twist did not provide an optimum angle of attack distribution in cruise.

Reducing root airfoil thickness had a major effect on cruise performance, but little effect on hover figure of merit. Increasing tip airfoil thickness did not improve figure of merit, and reduced propulsive efficiency despite the low tip speed.

Recommendations

Aeroelastic stability has yet to be examined in detail. While a shortfall in performance would be disappointing, an instability would be fatal to the concept. The LCTR2 structure is scaled from LCTR1, so no problems are anticipated. On the other hand, failure to recognize and exploit improved stability margins would result in reduced performance and unnecessary weight. The impact on stability of a slowed proprotor combined with large size merits deeper exploration and should be given high priority.

Several options are herein proposed for improved and extended design optimization. However, the optimization process itself needs refinement. Perhaps the most important change would be to more thoroughly integrate maneuver requirements into rotor optimization. Selection of solidity would then be bounded by the required maneuver capability. Calculation of performance in maneuvers, especially turns, is much more computationally demanding than hover or cruise in axial flow, so development of a simplified analysis is appropriate. An additional improvement would be to develop an explicit cost function to more closely connect rotor performance optimization to overall mission capability. With some combinations of solidity, taper, and tip speed, rotor performance proved very sensitive to twist, which implies that a range of operating conditions

may have to be analyzed to avoid over-optimization at the nominal design point.

The specification of thrust capability in hover, cruise, and maneuvers needs closer attention to ensure proper design tradeoffs. The implicit assumptions of rotor aerodynamics technology, including airfoils, merit revision, commensurate with the assumed service entry date.

As the rotor is slowed in cruise, the traditional methods of specifying twist, taper, and airfoil distribution may require revision. Bilinear twist has been standard practice since the debut of the XV-15 three decades ago. Analytical methods now exist for detailed examination and optimization of nonlinear twist, which is highly recommended. Nonlinear taper also deserves exploration.

The tradeoffs between tip and root airfoil thickness, tip speed, and performance have barely been touched upon. The high sensitivity to root thickness suggests that the root deserves closer attention than the tip.

Acknowledgments

References

1. Johnson, W., Yamauchi, G. K., and Watts, M. E., "Designs and Technology Requirements for Civil Heavy Lift Rotorcraft," AHS Vertical Lift Aircraft Design Conference, San Francisco, California, January 2005.

2. Johnson, W., Yamauchi, G. K., and Watts, M. E., "NASA Heavy Lift Rotorcraft Systems Investigation," NASA TP-2005-213467, September 2005.

3. Acree, C. W., and Johnson, W., "Performance, Loads and Stability of Heavy Lift Tiltrotors," American Helicopter Society Vertical Lift Aircraft Design Conference, San Francisco, California, January 2006.

4. van Aken, J. M. and Sinsay, J. D., "Preliminary Sizing of 120-Passenger Advanced Civil Rotorcraft Concepts," AHS Vertical Lift Aircraft Design Conference, San Francisco, California, January 2006.

5. Johnson, W., Yeo, H., and Acree, C.W., "Performance of Advanced Heavy-Lift, High-Speed Rotorcraft Configurations," AHS International Forum on Rotorcraft Multidisciplinary Technology, Seoul, Korea, October 2007.

6. Acree, C. W., "Impact of Technology on Heavy Lift Tiltrotors," American Helicopter Society 62nd Annual Forum, Phoenix, Arizona, May 2006.

7. Coy, J. J., "Cost Analysis for Large Civil Transport Rotorcraft," AHS Vertical Lift Aircraft Design Conference, San Francisco, California, January 2006.

8. Johnson, W., "CAMRAD II Comprehensive Analytical Model of Rotorcraft Aerodynamics and Dynamics," Johnson Aeronautics, Palo Alto, California, 2005.

9. Zhang, J., and Smith, E., "Design Methodology and Cost Analysis of Composite Blades for a Low Weight Rotor," AHS Vertical Lift Aircraft Design Conference, San Francisco, California, January 2006.

10. Du, Z., and Selig, M.S., "A 3-D Stall-Delay Model for Horizontal Axis Wind Turbine Performance Prediction," AIAA Paper 98-0021, January 1998.

11. Acree, C. W., "Calculation of JVX Proprotor Performance and Comparisons with Hover and High-Speed Test Data," AHS Specialist's Conference on Aeromechanics, San Francisco, California, January 2008.

12. Acree, C. W., "Modeling Requirements for Analysis and Optimization of JVX Proprotor Performance," AHS 64th Annual Forum, Montréal, Canada, April 2008.

13. Narramore, J. C., "Airfoil Design, Test, and Evaluation for the V-22 Tilt Rotor Vehicle," 43rd Annual Forum of the American Helicopter Society, St. Louis, Missouri, May 1987.

14. Acree, C. W., Martin, P. B., and Romander, E. A., "Impact of Airfoils on Aerodynamic Optimization of Heavy Lift Rotorcraft," American Helicopter Society Vertical Lift Aircraft Design Conference, San Francisco, California, January 2006.

15. Martin, P. B., Rhee, M., Maughmer, M. D., and Somers, D. M., "Airfoil Design and Testing for High-Lift Rotorcraft Applications," AHS Specialist's Conference on Aeromechanics, San Francisco, California, January 2008.

16. Dadone, L., Liu, J., Wilkerson, J., and Acree, C. W., "Proprotor Design Issues for High Speed Tiltrotors," American Helicopter Society 50th Annual Forum, Washington, D.C., May 1994.

17. Yeo, H., and Johnson, W., "Performance and Design Investigation of Heavy Lift Tiltrotor with Aerodynamic Interference Effects," American Helicopter Society 63rd Annual Forum, Virginia Beach, Virginia, May 2007.

18. Narramore, J. C., Platz, D. A., and Brand, A. G., "Application of Computational Fluid Dynamics to the Design of the BA 609," 25th European Rotorcraft Forum, Rome, Italy, September 1999.